An Alfvén Eigenmode Similarity Experiment

W.W. Heidbrink, Y. Luo,
University of California, Irvine
E. Fredrickson, N.N. Gorelenkov, G. Kramer
Princeton Plasma Physics Laboratory
A.W. Hyatt
General Atomics

ABSTRACT.

The major radius dependence of Alfvén mode stability is studied by creating plasmas with similar minor radius, shape, magnetic field (0.5 T), density ($n_e \simeq 3 \times 10^{19}$ m^{-3}), electron temperature (1.0 keV) and beam-ion population (near-tangential 80 keV deuterium injection) on both NSTX and DIII-D. The major radius of NSTX is half the major radius of DIII-D. The super-Alfvénic beam ions that drive the modes have overlapping values of v_f/v_A in the two devices. Observed beam-driven instabilities include toroidicity-induced Alfvén eigenmodes (TAE). The stability threshold for the TAE is similar in the two devices. As expected theoretically, the most unstable toroidal mode number n is larger in DIII-D.

1. Introduction

In a cylinder, solutions of the dispersion relation $\omega = k_{\|} v_A$ for shear Alfvén waves exist for all values of the frequency ω below the ion cyclotron frequency Ω but, in a torus, a gap exists in the frequency spectrum that grows wider with the ratio of the minor radius to the major radius, a/R [1]. The toroidicity-induced Alfvén eigenmode (TAE) is a radially extended normal mode of the plasma with a frequency that falls in this spectral gap [2]. In the first experimental observations of the TAE, 80-110 keV deuterium neutrals were injected into low-field tokamak plasmas to create super-Alfvénic beam ion populations that drove the mode unstable [3, 4]. Subsequent experiments established that the mode can be excited by external antennas [5] and a wide variety of energetic ion populations [6], including alpha particles created in deuterium-tritium (DT) reactions [7].

The energetic alpha population in a DT tokamak reactor may drive the TAE unstable, particularly if the reactor operates with weak magnetic shear or at temperatures above 20 keV [8]. It is widely anticipated that the most unstable toroidal mode numbers n in a reactor will be higher than in current experiments [8, 9]. For n =15-25, the stability threshold is fairly insensitive to toroidal mode number so, if the TAE is unstable, many modes will probably be excited. Observations of TAEs excited by ion cyclotron heating support this expectation: when modes with $n \simeq 10$ are observed, many other toroidal mode numbers are usually observed simultaneously [10, 11]. In a reactor, with a "sea" of unstable modes driven unstable by an isotropic alpha particle population, the dominant mode saturation mechanism may differ from the mechanisms that operate in current experiments.

Theoretically, the expectation of high toroidal mode numbers in a reactor is based on the idea that the energy extracted from the fast ions decreases when the orbit size exceeds the mode width. Numerical studies indicate that the largest fast-ion drive is expected when $k_\theta \rho_f \simeq 1$ [12], where k_θ is the poloidal wave number of the TAE and ρ_f is the toroidal gyroradius of the fast ions. Reexpressing this prediction in terms of n, the most unstable toroidal mode number n_{max} is approximately

$$n_{max} \simeq a B_T Z_f / (q\sqrt{8 E_f m_f}), \tag{1}$$

where B_T is the toroidal field, q is the safety factor, and Z_f, E_f, and m_f are the charge, energy, and mass of the fast ions. Analytical theory [13] predicts a plateau regime for the fast-ion drive when the poloidal mode number m is

of order $a\Omega_f/(qv_A)$, which implies a most unstable n of

$$n_{max} \simeq \frac{a(Z_f e)\sqrt{\pi m_i n_e/m_f^2}}{cq^2} \tag{2}$$

in cgs units. For $v_f \simeq v_A$, Eqs. 1 and 2 only differ by a factor of q; neither expression depends explicitly on the major radius. (The expected n_{max} in a reactor is large because aB_T is large.) Experimental confirmation of either prediction is scanty. An inter-machine comparison of observations from several tokamaks shows rough agreement with the prediction of Eq. 1 [14]. Also, on an individual machine, n_{max} usually increases with toroidal field and decreases with safety factor.

Equations 1 and 2 are based on the dependence of the fast-ion drive on toroidal mode number. In reality, instability is determined by the *competition* between the fast-ion drive and the mode damping rate. Damping rates can depend sensitively on toroidal mode number, especially when n is small and the radial mode structure is large. Some damping mechanisms, such as Landau damping on the thermal ion population, are insensitive to n while others, such as coupling to strongly damped modes, depend sensitively on the radial eigenfunction.

One goal of the present experiment is to test the validity of Eqs. 1 and 2. A second objective is to relate TAE stability in a spherical tokamak (ST) to TAE stability in a conventional tokamak. In a spherical tokamak, the minor radius is comparable to the major radius. In frequency space, the "gap" associated with toroidicity becomes *wider* than the portion spanned by the Alfvén continuum. Two posited damping mechanisms, continuum [15, 16] and radiative [17] damping, involve coupling between the gap mode and the continuum. If these mechanisms are important, the ST could be more unstable than conventional tokamaks.

The National Spherical Torus Experiment (NSTX) and the DIII-D tokamak are nearly ideal for an Alfvén mode similarity experiment. Both devices use tangentially injected 80-keV deuterium neutral beams to heat the plasma. DIII-D is able to match the low toroidal field employed on NSTX, making it possible to match the most important dimensionless parameter for Alfvén mode stability, the ratio of fast-ion speed to Alfvén speed, v_f/v_A. The dimensionless fast-ion pressure, β_f, is also similar in the two devices. In addition, the cross-sectional shapes of the plasmas can be closely matched. Thus, it is possible to study TAEs with all plasma parameters closely matched except the major radius, which differs by a factor of two in the two devices.

The results of this study indicate that the stability properties of the ST and a conventional tokamak are similar in this regime. The most unstable toroidal mode number n_{max} is higher in DIII-D than in NSTX, as predicted by Eq. 1.

2. Experimental Conditions

NSTX is a low toroidal field tokamak. Since typical densities in NSTX and DIII-D are comparable, in order to match the Alfvén speed $v_A = B/\sqrt{\mu_0 n_i m_i}$ in the two devices, DIII-D is operated at much lower toroidal fields than usual, B_T = 0.5-0.6 T. This is still larger than the vacuum NSTX toroidal field of $\sim$ 0.43 T but, because of the large paramagnetic contribution to the toroidal field in a ST, the average value of B_T at the magnetic axis in NSTX is 0.53 T for these experiments. The angles of beam injection are shown in Fig. 1. In DIII-D, two injection angles are available: the Left beams with tangency radii of R_{tan} = 1.15 m and the Right beams with R_{tan} = 0.76 m. In NSTX, the beams inject at tangency radii of 0.69 m (Source A), 0.59 m (Source B), and 0.49 m (Source C). In the experiment, different sources are employed. To approximately match the average pitch $v_{\|}/v_f$ of the beam populations, the Left DIII-D source is compared with either NSTX Source A or B and the Right DIII-D source is compared with NSTX Source C. To approximately match the fraction of beam ions that are on banana orbits (the trapped/passing fraction), the Right DIII-D source is compared with NSTX source A.

The achieved cross-sectional shapes of the plasma are close but not identical (Fig. 2). To achieve an overlapping range of densities, two boundary configurations are employed on both machines: a plasma that is limited on the inner graphite wall and a double-null divertor configuration with a small ($\lesssim$2 cm) inner gap. Typically, the minor radius is a = 0.60 m, the elongation is κ = 1.75 and the triangularity is δ = 0.4. Avoidance of the outer baffle plates on DIII-D creates a flattened outer surface at poloidal angles of $270 \pm 45^\circ$ that cannot be matched exactly with the available NSTX shaping coils. The conditions included in the database of Sec. 3 include minor radii between 0.58-0.62 on DIII-D and 0.55-0.65 on NSTX, elongations between 1.5-1.85 on DIII-D and 1.5-2.3 on NSTX, and triangularities between 0.2-0.5 on DIII-D and 0.3-0.8 on NSTX. Empirically, modest changes in shape about the target shape have little (if any) effect on the beam-driven instabilities. As desired, the major difference in the two devices is the major radius: R_0 = 0.88 m on NSTX and R_0 = 1.70 m on DIII-D.

With the minor radius, toroidal field, and beam parameters matched, the plasma current I_p is the remaining operational variable. TAE stability depends on both the q profile and the fast-ion orbital size but it is impossible to match both of these simultaneously in an aspect-ratio scaling study. In both devices, the beam ion orbits span a significant fraction of the minor radius (Fig. 3). To minimize prompt beam-ion losses, operation above $I_p \simeq 0.6$ MA is desirable. This condition is readily achieved in NSTX but is problematic in DIII-D because the edge safety factor approaches three; also, at low q, the sawtooth inversion radius becomes quite large and redistribution of the beam ions at the sawtooth crash has a strong effect on the fast-ion-driven instabilities. For these experiments, the average value of plasma current is 0.55 MA in DIII-D, spanning a range of 0.35-0.68 MA. The average value of plasma current is 0.98 MA in NSTX, spanning a range of 0.66-1.18 MA.

Internal measurements of the magnetic field are currently unavailable on both devices in this parameter regime. The equilibria are determined from EFIT reconstructions [18] using external magnetics measurements. For DIII-D, soft x-ray measurements of the sawtooth inversion radius provide an internal constraint on the q profile; for NSTX, the standard fitting procedure is based on the assumption that $q_0 = 1$ when sawteeth begin.

Thomson scattering measurements [19, 20] of the electron temperature and density are the principal plasma diagnostic in both devices. The relatively low central electron temperature of $T_e \lesssim 1$ keV implies that, classically, beam ions slow down primarily on thermal electrons. Accordingly, the classical pitch-angle scattering rate is an order of magnitude smaller than the energy deceleration rate. Under these conditions, the ion temperature and plasma rotation (which are unavailable for most of the discharges) have little effect on the classical beam-ion confinement or neutron rate. The Alfvén speed v_A is usually larger than the critical speed v_{crit} where ion and electron drag are equal, v_A/v_{crit} =1-2.

Typical discharges from each device are shown in Figs. 4 and 5. Since the primary objective of the study is to determine the linear stability of the TAE, the beam power is modest in both devices. In previous low-field TAE studies on DIII-D, the transition from TAE activity to "Beta-induced Alfvén Eigenmode" (BAE) activity occurred when the power was increased from 5 MW to 7.5 MW [21]. In this study, the beam power in DIII-D is restricted to $P_B \lesssim 2.5$ MW. In NSTX, no more than one source ($P_B \simeq 1.5$ MW) is injected and, in many cases, the source is modulated to give a more precise determination of the stability threshold. At these modest powers, the total

plasma beta is too small to create a magnetic well (which could significantly alter the beam-ion orbits). Fast-ion transport by the instabilities is also minimized at these low beam powers. In NSTX, the ratio of the measured neutron rate to the classically-expected rate is unaffected by the appearance of beam-driven instabilities. In DIII-D, the neutron rate is $\sim 15\%$ lower than expected in the discharges with strong TAE activity.

In the double-null divertor DIII-D discharges, a transition to the H-mode often occurs. For example, in the discharge shown in Fig. 4, a transition occurs following the sawtooth crash around 0.90 s and the density begins to increase. Increasing density causes a reduction in the Alfvén speed, which is reflected in the gradual decrease in the nominal TAE frequency $v_A/(4\pi qR)$ and in the beam pressure (not shown). TAE activity is evident at the end of the sawtooth cycle. The modes are transiently stable after each sawtooth crash, presumably because of flattening of the q profile [22], of the beam-ion pressure profile, or both. Most of the DIII-D discharges eventually disrupt. Discharges with lower beam voltage (and power) persist longer.

In NSTX, beam injection commences earlier in the discharge (Fig. 5). Although the density steadily rises, the nominal TAE frequency usually increases because q continues to fall as the discharge evolves. (The radius of the maximum value of $d\beta_{fast}/dr$ evolves more gradually.) If the beam power is modulated, the neutron rate rises and falls. Bursts of beam-driven instabilities are more likely when the beam population is largest (near the peaks in the neutron rate). A wide variety of beam-driven instabilities are observed, including modes with frequencies comparable to the expected TAE frequency and modes with frequencies closer to the ion cyclotron frequency that are probably compressional Alfvén eigenmodes (CAE) [23]. Later in the discharge, the instabilities often disappear as the density rises and the beam pressure declines.

To analyze the data, the magnetic activity is classified and a database is compiled from all of the discharges acquired during the two days of dedicated experiments. For example, in the example shown in Fig. 4, the activity at 1.04 s is classified as "unstable" activity, while the activity around 1.18 s is only occasionally detectable, so this time slice is classified as "weak" activity. Because reliable internal measurements that span the plasma are unavailable, the most unstable toroidal mode n_{max} is assumed to be the mode with the largest amplitude in the magnetics spectra. Although this is the most reasonable interpretation of the available measurements, it is not necessarily correct. If the eigenfuntions of the various modes differ appreciably, a dif-

ferent mode could have the largest internal amplitude. Also, the maximum mode amplitude occurs after nonlinear saturation, which could have a different n dependence than the linear stability properties.

Figure 6 shows the profiles of T_e, n_e, and q for all of the timeslices that have unstable TAE activity. Usually, the electron temperature is lower, the electron density is comparable, and the safety factor is larger in NSTX than in DIII-D. The central q exceeds 1.5 in only a single DIII-D discharge with early beam injection, while $q_0 < 1.5$ is rare in NSTX.

3. Empirical Results

The beam-driven instabilities exhibit greater variety on NSTX than on DIII-D. Although there are indications of CAE activity on some DIII-D discharges, CAE are observed on most of the NSTX discharges. There is also more variety in the frequency band around the TAE. Figures 5 and 7 show representative examples. The frequency of some modes chirps down rapidly by 30 kHz or more on a 1 ms timescale. For other modes, if chirping occurs, it happens too rapidly to resolve in a Fourier transform but a broad, 10-kHz wide, spectral line is evident. In other cases, the linewidth is narrow (comparable to the instrumental resolution of ~ 1 kHz). In contrast, in DIII-D, the linewidth of all of the beam-driven instabilities is narrow (Fig. 8).

The relationship of these various modes to the TAE is uncertain. The rapidly chirping mode is probably a type of energetic particle mode [24, 25], perhaps the resonant-TAE [26]. The $n = 1$ mode with the ~ 10 kHz linewidth may be a bounce-resonance fishbone [27]. Alternatively, the linear instability may be the same in the various cases but the nonlinear saturation mechanisms may show greater variety than in a conventional tokamak; for example, the broad line may be associated through the uncertainty principle with the very short duration of the bursts, $\delta f \sim 1/\delta t \simeq 1/(0.1 \text{ ms}) = 10$ kHz. In any event, for the purposes of this comparative study, we adopt the following conservative definition of a TAE.

- The mode frequency lies in the TAE gap.
- The linewidth is narrow.
- Multiple n numbers appear simultaneously.

The latter criterion is chosen because a "cluster" of toroidal modes separated by the Doppler shift is a common signature of TAEs in DIII-D [28]. Moreover, less sensitivity to toroidal mode number is expected for the TAE than for

the bounce-resonance fishbone [29]. Figure 9 shows representative examples of spectral clusters that qualify as TAEs.

Data from poloidal arrays of magnetic probes show that the modes have the expected ballooning structure (Fig. 10a). The phase changes more gradually with poloidal angle in NSTX than in DIII-D, as expected for a mode with a smaller poloidal wavenumber (Fig. 10b).

The stability properties of the data are summarized in Fig. 11. Although the NSTX data have a higher average value of v_f/v_A than the DIII-D data, the experiment successfully acquired overlapping values. The TAE stability properties correlate more strongly with beam beta than with other plasma parameters. Empirically, the threshold is comparable in the two devices. Injection of a single, super-Alfvénic neutral beam source normally gives instability.

Higher toroidal mode numbers are observed in DIII-D than in NSTX (Fig. 12a). In NSTX, virtually all of the TAE clusters have $n_{max} = 1$ while, in DIII-D, the strongest line in the cluster is usually $n_{max} = 5$. Within the framework of Eq. 1, the cause of this difference is the higher q in NSTX, not the smaller major radius. The correlation between experiment and theory is equally good with Eq. 1 and 2, so it is not possible to distinguish between q^{-1} or q^{-2} scaling of n. As predicted by Eq. 2, the toroidal mode number correlates with n_e. The discharge with early beam injection and elevated values of central q has the lowest values of n_{max} observed in DIII-D.

The data from this experiment extend the range of a previously compiled inter-machine database (Fig. 12b). The simple scaling law (Eq. 1) approximately describes the observations.

4. Theoretical Analysis

Unstable discharge conditions from each machine are selected for detailed theoretical analysis. The plasma profiles, including the classically expected beam-ion distribution function, are calculated from experimental data using the TRANSP analysis code [30]. The selected condition for DIII-D follows an H-mode transition, so the density profile is broader and the electron temperature is higher than in the NSTX condition (Fig. 13). The safety factor in NSTX is about twice as large as in DIII-D. The beam sources are the Right beam in DIII-D and Source B in NSTX, so the fraction of trapped beam ions is slightly higher in NSTX but the ratio of perpendicular to parallel beam energy is higher in DIII-D. The profile of the toroidal beam beta is very similar in the two machines, although the poloidal beam beta is higher in DIII-D because the plasma current is lower. In both devices, the beam

pressure constitutes a significant fraction of the total pressure.

A large frequency gap exists in the Alfvén continuum for both devices (Fig. 14a and b). As expected, the continuum is virtually non-existent in NSTX near the plasma edge where $a \simeq R$. Experimentally, in DIII-D, there is a TAE cluster with toroidal mode numbers of 4-7 at this time. The frequency of the strongest mode, the $n = 6$, is $f_{lab} = 108$ kHz in the laboratory frame. For most of the bursts of TAE activity around this time, $n = 6$ is the strongest toroidal mode but the $n = 4$ peak is largest on a few of the bursts. Assuming that the peak splitting Δf is caused primarily by the Doppler shift and that the various toroidal modes are excited at similar radial positions [28], the mode frequency in the plasma frame is $f_{pl} \simeq f_{lab} - n\Delta f = 43$ kHz. For the NSTX case, the $n = 1$ mode is largest and the inferred frequency in the plasma frame is $f_{pl} = 70$ kHz.

NOVA-K [31] is a global code that calculates the MHD eigenfunction. The calculated frequencies of unstable TAEs are acceptably close to the measured values for both cases (Fig. 14a and b). The calculated eigenfunction is broad in both devices, especially in NSTX (Fig. 14c and d).

NOVA-K computes TAE stability perturbatively. For this analysis, the distribution function is modeled as Gaussian in pitch angle and slowing down in velocity, with the radial density dependence calculated by TRANSP. The computed value of collisional damping by electrons is unphysically large for these discharges, perhaps due to a deficiency in the model at low aspect ratio. The computed radiative damping is comparable in magnitude to the computed fast-ion drive term but the model is of questionable validity for such large spectral gaps. The electron and ion Landau damping terms are both of $O(0.01\omega_A)$ but the uncertainty in the ion Landau damping term is large because reliable T_i profiles are unavailable. The computed beam-ion drive term is largest for $n = 1$ in NSTX (Fig. 15), in agreement with the experimental observation that the $n = 1$ mode is most unstable. For DIII-D, the drive term is largest for $n = 4$, with similar values for $n = 3$ and $n = 5$. Experimentally, $n_{max} = 6$ in this discharge.

Analysis with the HINST [32] code is complementary to analysis with NOVA-K. An advantage of HINST is that it is a non-perturbative fully kinetic code, which is important for such intense fast-ion populations; however, the code computes stability locally based on a high n formalism, which is inappropriate for large global eigenfunctions. Only the contribution to the fast-ion drive of the passing particles is considered here. Calculations of the expected mode frequencies and growth rates are shown as a function of posi-

tion in Fig. 16. Unstable modes in the TAE gap are predicted for both cases. Figure 17 shows the frequency and growth rate as a function of toroidal mode number. For NSTX, HINST predicts instability for both $n = 1$ and $n = 2$, with $n = 2$ the most unstable mode. (Experimentally, both are observed but $n_{max} = 1$ on the magnetic probe.) For DIII-D, the predicted growth rate is similar for n = 3-6, in reasonable agreement with the experimental results.

5. Discussion and Conclusion

It is possible to operate DIII-D with magnetic fields and a cross-sectional shape that is similar to normal NSTX operation. Since the neutral beam injectors are nearly identical, these two devices are well suited for experimental tests of the aspect-ratio dependence of beam-driven instabilities. In addition to TAEs (the focus of this study), CAEs are also observed in both devices. A comparison of their properties is a topic for future experiments.

Beam-driven modes with frequencies that rapidly chirp are extremely common on NSTX. The basic properties of these chirping modes are the same as the DIII-D "chirping modes" reported in Ref. [33]: $f \simeq \frac{1}{2} f_{TAE}$, $\delta f/f \sim 50\%$, burst duration of $\sim$ 1 ms, toroidal mode numbers of n = 1, 2, and 3. (Similar instabilities are observed in other conventional [34] and spherical [35] tokamaks.) A major difference, however, is that these modes are rare in DIII-D, occurring in $\lesssim$1% of the discharges with beam-driven instabilities. Another difference between NSTX and DIII-D is the relatively broad linewidth of instabilities with no apparent chirping (such as the mode with the $\sim$ 10 kHz linewidth shown in Fig. 7). Further experiments and theory are needed to understand these phenomena.

For the TAE with a narrow linewidth, the stability threshold is comparable in the two devices. Theoretically, both NOVA and HINST predict that NSTX should be a little more unstable than DIII-D. A global, non-perturbative calculation of TAE stability for these cases is desirable. As a preliminary conclusion, despite the wide gaps in the Alfvén continuum, ST stability to fast-ion driven modes is no worse than conventional tokamak stability.

An earlier compilation [14] of independently published measurements from several tokamaks found rough agreement with the simple scaling law for the most unstable toroidal mode number, Eq. 1. In this study, discharges with carefully matched plasma and beam parameters also agree with Eq. 1. These results strengthen the expectation that, if Alfvén modes are driven unstable by alpha particles in a reactor, many modes with n = 10-20 will appear.

ACKNOWLEDGEMENTS

The assistance of S. Bernabei, Liu Chen, G.Y. Fu, D. Gates, D. Mueller, T. Rhodes, and the entire NSTX and DIII-D team is gratefully acknowledged. This work was funded by the U.S. Department of Energy.

References

[1] GLOEDBLOED, J. P., Phys. Fluids **18** (1975) 1258.

[2] CHENG, C. Z., CHEN, L., and CHANCE, M., Annals Physics **161** (1985) 21.

[3] WONG, K. L., FONCK, R. J., PAUL, S. F., et al., Phys. Rev. Lett. **66** (1991) 1874.

[4] HEIDBRINK, W. W., STRAIT, E. J., DOYLE, E., SAGER, G., and SNIDER, R. T., Nucl. Fusion **31** (1991) 1635.

[5] FASOLI, A., BORBA, D., BOSIA, G., et al., Phys. Rev. Lett. **75** (1995) 645.

[6] WONG, K.-L., Plasma Phys. Controlled Fusion **41** (1999) R1.

[7] NAZIKIAN, R., FU, G. Y., BATHA, S. H., et al., Phys. Rev. Lett. **78** (1997) 2976.

[8] GORELENKOV, N. N., BERK, H. L., BUDNY, R., et al., Nucl. Fusion **43** (2003) submitted.

[9] ITER Physics Expert Group on Energetic Particles, Heating, and Current Drive et al., Nucl. Fusion **39** (1999) 2471.

[10] SAIGUSA, M., KIMURA, H., KUSAMA, Y., et al., Plasma Phys. Controlled Fusion **40** (1998) 1647.

[11] FASOLI, A., BORBA, D., GORMEZANO, C., et al., Plasma Phys. Controlled Fusion **39** (1997) B287.

[12] FU, G. Y. and CHENG, C. Z., Phys. Fluids B **4** (1992) 3722.

[13] BREIZMAN, B. N. and SHARAPOV, S. E., Plasma Phys. Controlled Fusion **37** (1995) 1057.

[14] HEIDBRINK, W. W., Phys. Plasmas **9** (2002) 2113.

[15] ROSENBLUTH, M. N., BERK, H. L., VAN DAM, J. W., and LINDBERG, D. M., Phys. Rev. Lett. **68** (1992) 596.

[16] ZONCA, F. and CHEN, L., Phys. Rev. Lett. **68** (1992) 592.

[17] METT, R. R. and MAHAJAN, S. M., Phys. Fluids B **4** (1992) 2885.

[18] LAO, L. L., ST. JOHN, H., STAMBAUGH, R. D., KELLMAN, A. G., and PFEIFFER, W. P., Nucl. Fusion **25** (1985) 1611.

[19] CARLSTROM, T. N., CAMPBELL, G. L., DEBOO, J. C., et al., Rev. Sci. Instrum. **63** (1992) 4901.

[20] LEBLANC, B. P., BELL, R. E., JOHNSON, D. W., et al., Rev. Sci. Instrum. **73** (2003) in press.

[21] HEIDBRINK, W. W., STRAIT, E. J., CHU, M. S., and TURNBULL, M. S., Phys. Rev. Lett. **71** (1993) 855.

[22] KRAMER, G. J., CHENG, C. Z., KUSAMA, Y., et al., Nucl. Fusion **41** (2001) 1135.

[23] FREDRICKSON, E. D., GORELENKOV, N., CHENG, C. Z., et al., Phys. Rev. Lett. **87** (2001) 145001.

[24] CHEN, L., Phys. Plasmas **1** (1994) 1519.

[25] BRIGUGLIO, S., KAR, C., ROMANELLI, F., VLAD, G., and ZONCA, F., Plasma Phys. Controlled Fusion **37** (1995) A279.

[26] CHENG, C. Z., GORELENKOV, N. N., and HSU, C. T., Nucl. Fusion **35** (1995) 1639, RTAE.

[27] FREDRICKSON, E. D., CHEN, L., and WHITE, R. B., Phys. Plasmas (2003) submitted.

[28] STRAIT, E. J., HEIDBRINK, W. W., and TURNBULL, A. D., Plasma Phys. Controlled Fusion **36** (1994) 1211.

[29] CHEN, L., (2002), private communication.

[30] BUDNY, R. V., Nucl. Fusion **34** (1994) 1247.

[31] CHENG, C. Z. and CHANCE, M. S., Phys. Fluids **29** (1986) 3695.

[32] GORELENKOV, N. N., CHENG, C. Z., and TANG, W. M., Phys. Plasmas **5** (1998) 3389, HINST.

[33] HEIDBRINK, W. W., Plasma Phys. Controlled Fusion **37** (1995) 937.

[34] KUSAMA, Y., KRAMER, G. J., KIMURA, H., et al., Nucl. Fusion **39** (1999) 1837.

[35] GRYAZNEVICH, M. P. and SHARAPOV, S. E., Nucl. Fusion **40** (2000) 907.

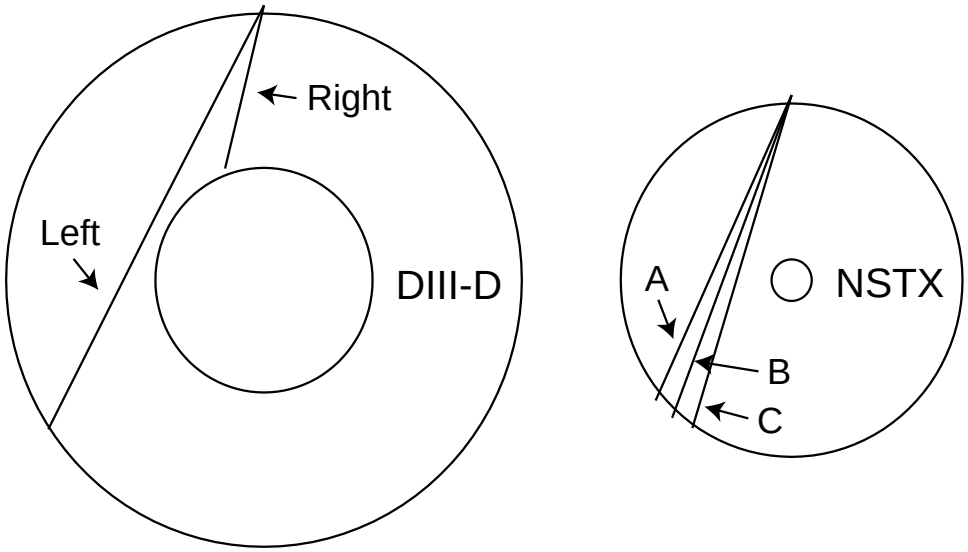

Figure 1. Plan views of the DIII-D and NSTX vacuum vessels at the horizontal midplane. The angles of injection for the Left and Right sources (DIII-D) and the A, B, and C sources (NSTX) are also shown.

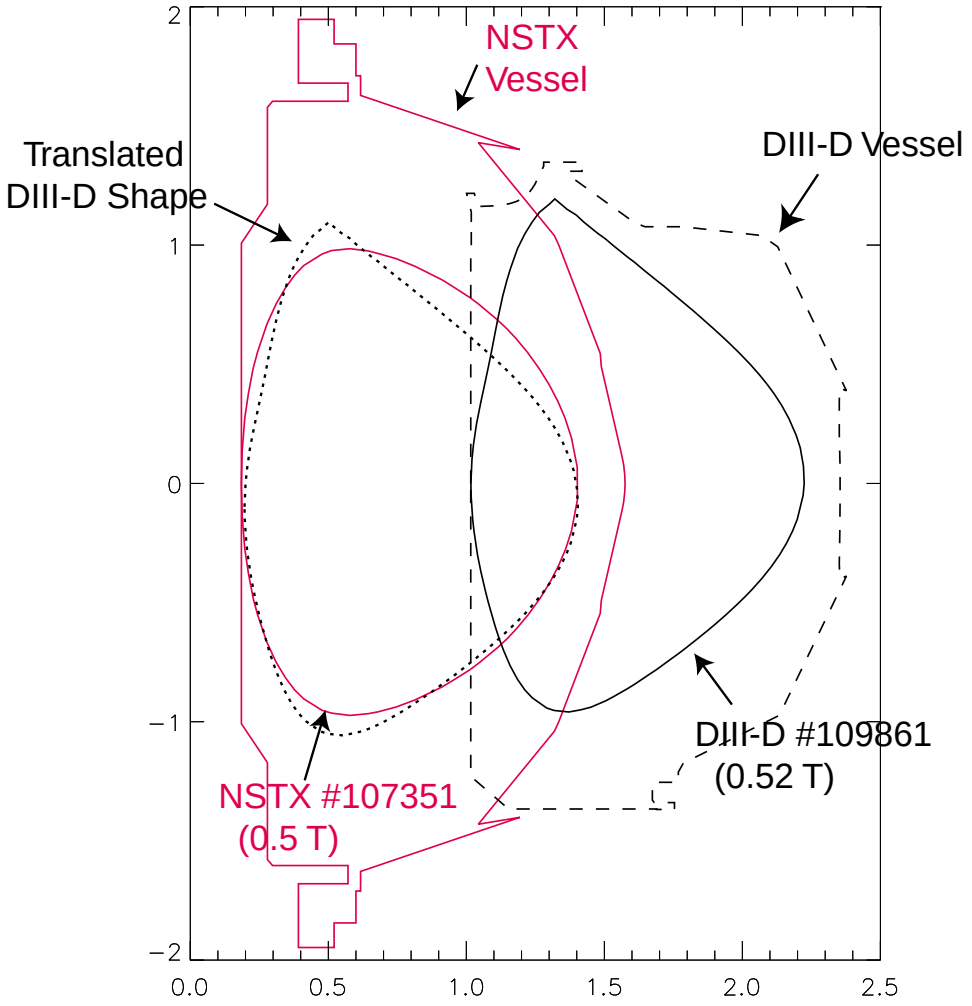

Figure 2. Elevation of the DIII-D and NSTX vacuum vessels and cross section of the last closed flux surface for two discharges from the experiment. An overlay of the DIII-D shape on the NSTX surface is also shown (dotted line).

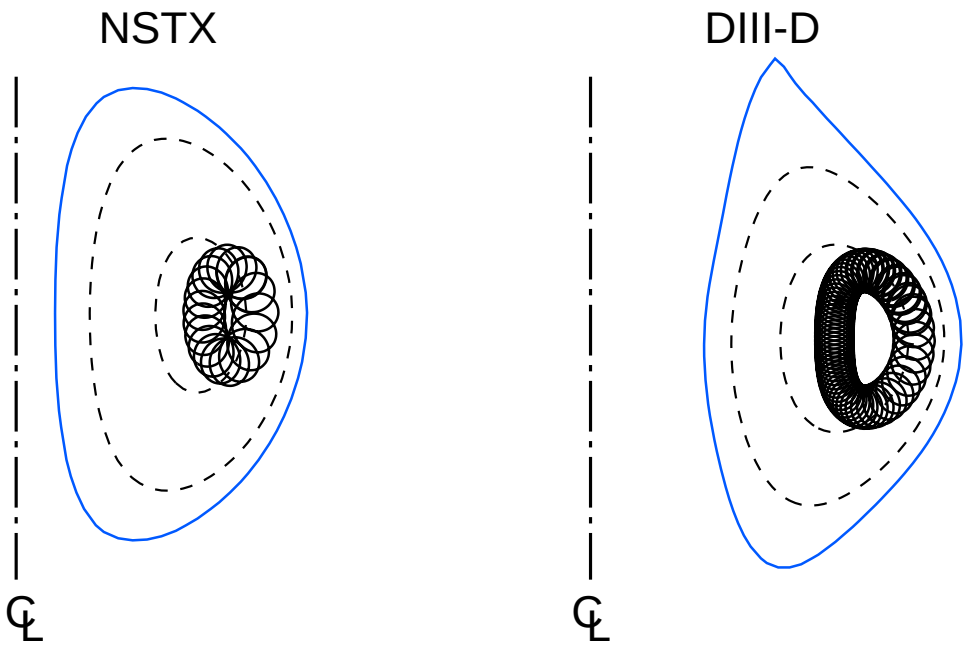

Figure 3. Poloidal projection of typical orbits of 80-keV deuterium beam ions injected by Source B into NSTX and by a Right source into DIII-D for the equilibria described in Fig. 13. The gyroradius and the shift of the drift orbit relative to the flux surface (dashed line) are both large.

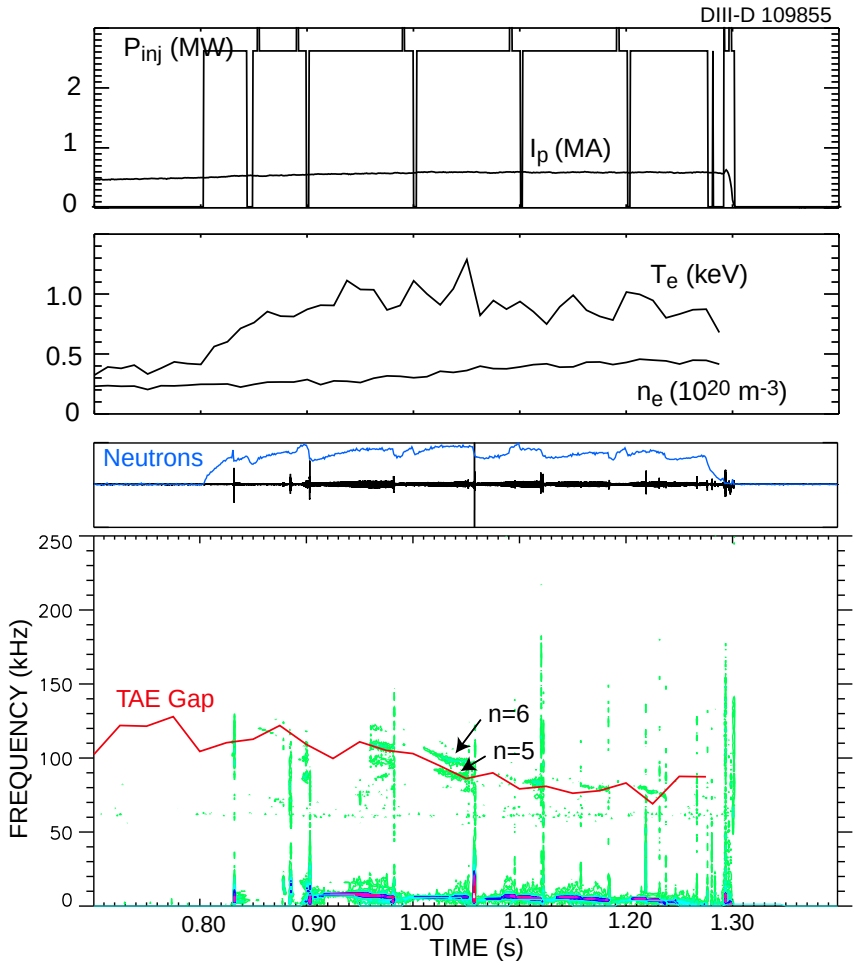

Figure 4. Injected beam power, plasma current, electron temperature and density near the plasma center, neutron rate, magnetics signal, and spectrogram from a pair of magnetics signals for one of the DIII-D discharges. The nominal frequency of the center of the TAE gap $v_A/(4\pi qR)$ (without Doppler shift correction) and the toroidal mode numbers of two of the modes are also shown. The vertical lines in the spectrogram are sawteeth. $B_T = 0.6$ T; double-null divertor configuration; 80-keV Right neutral beam source.

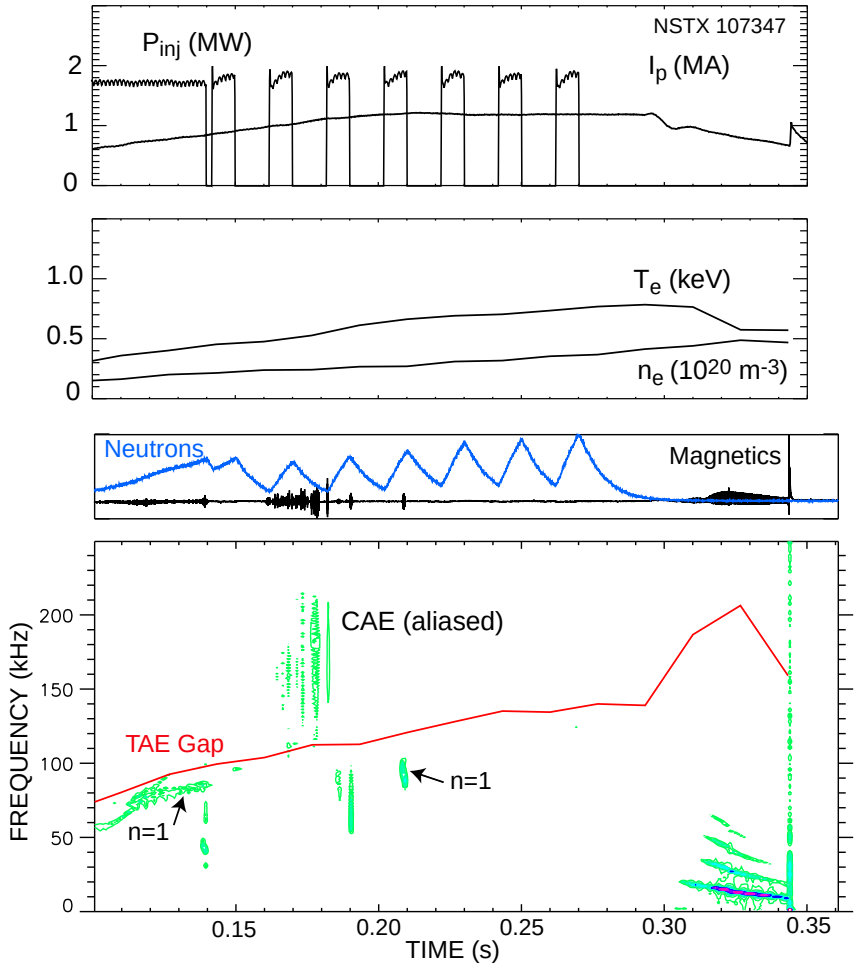

Figure 5. Injected beam power, plasma current, electron temperature and density near the plasma center, neutron rate, magnetics signal, and spectrogram from a pair of magnetics signals for one of the NSTX discharges. $B_T = 0.42$ T; inner-wall limiter configuration; Source B (A) before (after) 0.15 s.

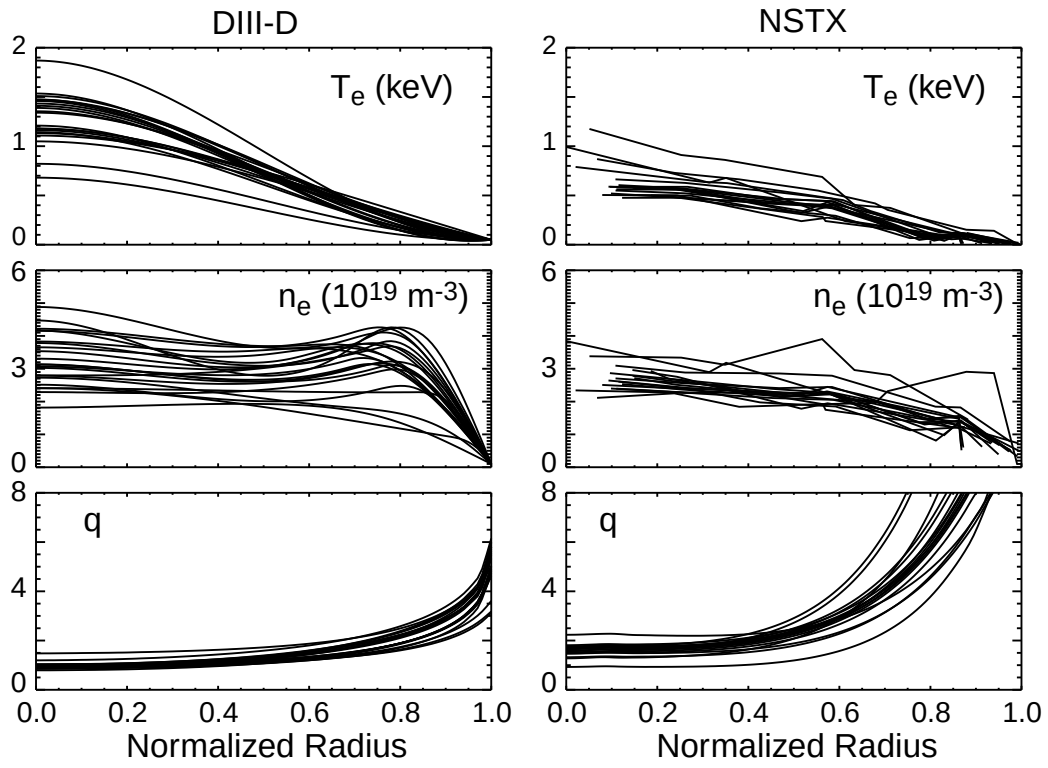

Figure 6. Thomson scattering profiles of electron temperature and density and EFIT reconstructions of the safety factor q for the DIII-D (left) and NSTX (right) discharges with TAE clusters. The Thomson profiles for DIII-D are from a spline fit to the data after mapping onto flux coordinates; the normalized radius is the square root of the toroidal flux. The Thomson profiles for NSTX are an approximate mapping of the raw data onto normalized minor radius.

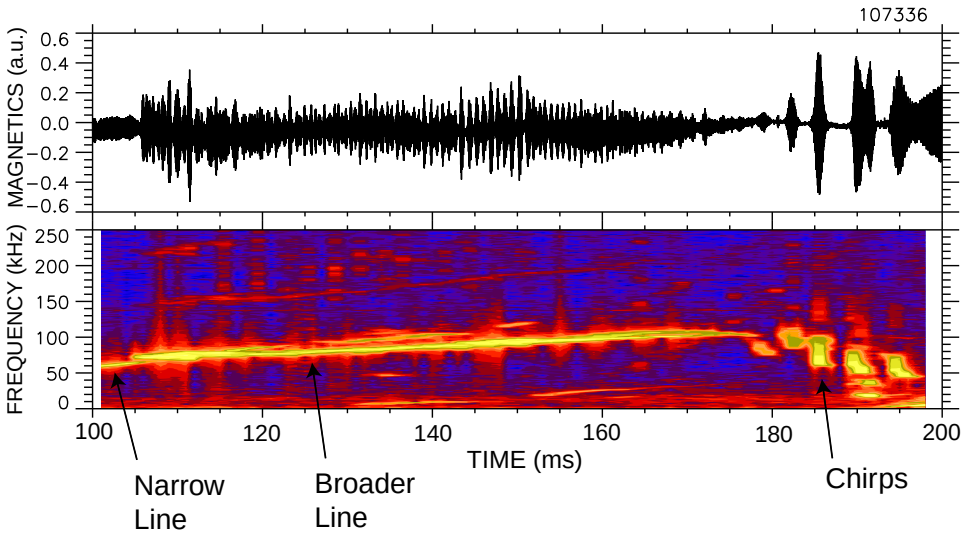

Figure 7. Magnetics signal and spectrogram from a pair of magnetic probes for an NSTX discharge with 1.7 MW of 81 kV deuterons injected by Source B. Linewidths of $\sim$ 2, 10, and 30 kHz are evident. $I_p = 0.93$ MA; $B_T(0) = 0.52$ T; $n_e \simeq 2.5 \times 10^{19}$ m^3; $T_e \simeq 0.52$ keV.

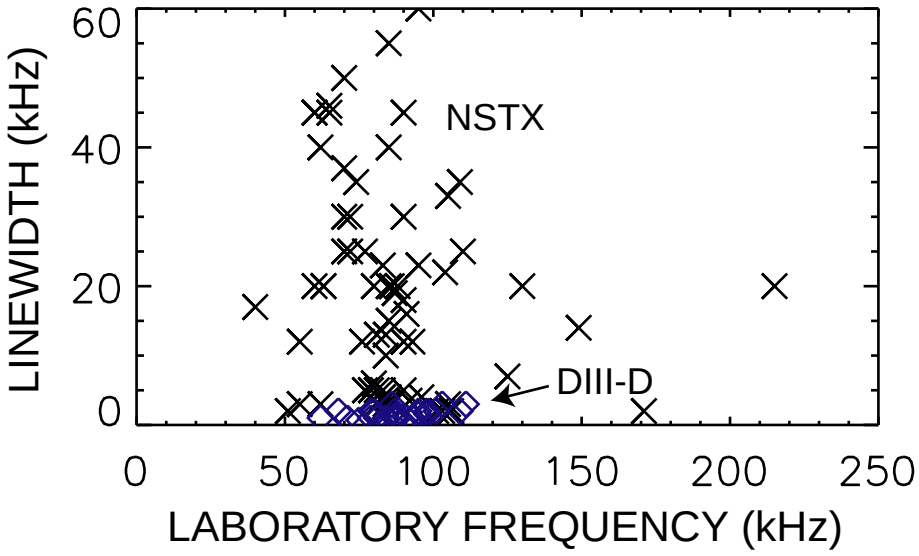

Figure 8. Linewidth δf of a 2-ms fast Fourier transform as a function of mode frequency for the database of NSTX discharges ($\times$) and DIII-D discharges ($\diamondsuit$).

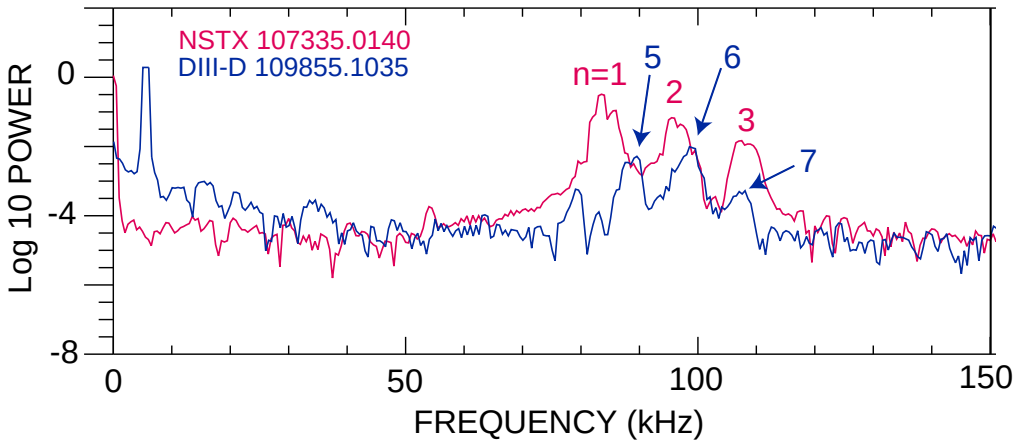

Figure 9. Spectra from a pair of magnetic probes in NSTX and in DIII-D. The toroidal modes of the peaks are indicated.

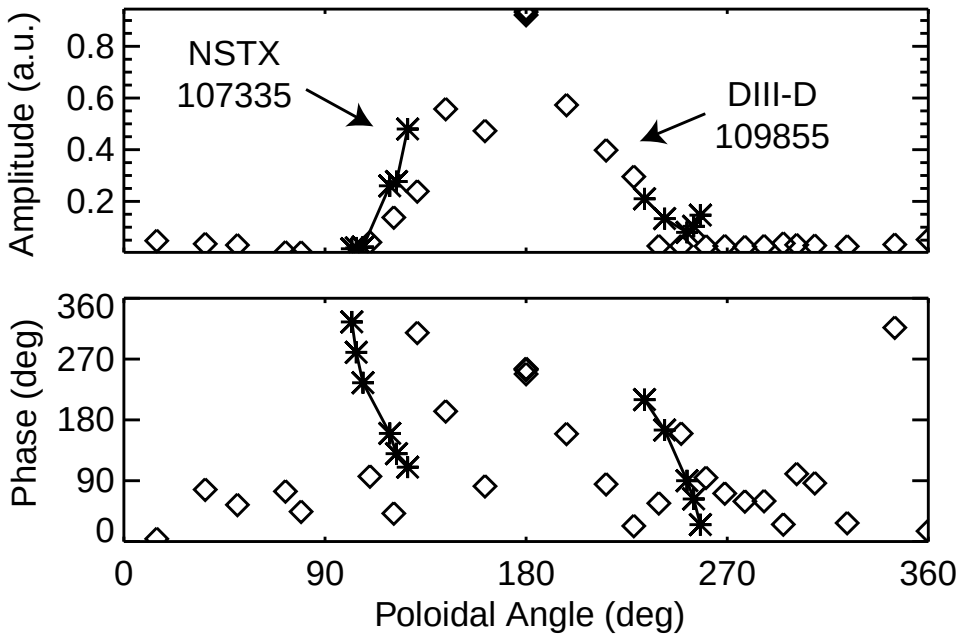

Figure 10. Amplitude (top) and phase (bottom) versus approximate poloidal angle for the poloidal arrays of magnetic probes in NSTX ($\times$) and DIII-D ($\diamondsuit$) for the $n = 1$ spectral peak at 0.139 s and 83.5 kHz and the $n = 6$ spectral peak at 1.035 s and 99 kHz shown in Fig. 9. The amplitude is largest at the outer midplane (180°), with the angle increasing in the clockwise direction.

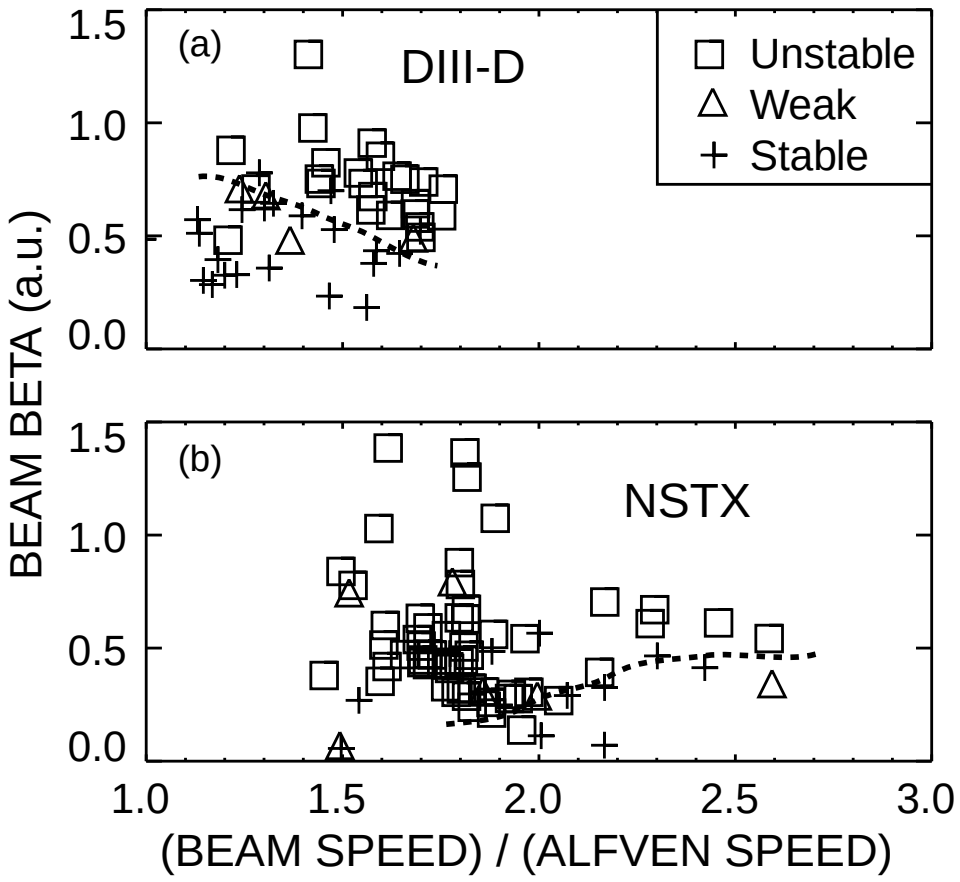

Figure 11. Beam beta versus v_f/v_A for the (a) DIII-D and (b) NSTX discharges in the database. The discharges are classified according to the strength of the TAE activity observed on the magnetics diagnostics; the dotted lines indicate the approximate empirical stability threshold. An approximate value of beam beta is derived from the relation $\beta_{beam} \propto (\text{Neutrons})/(n_e V B_T^2)$, where V is the plasma volume.

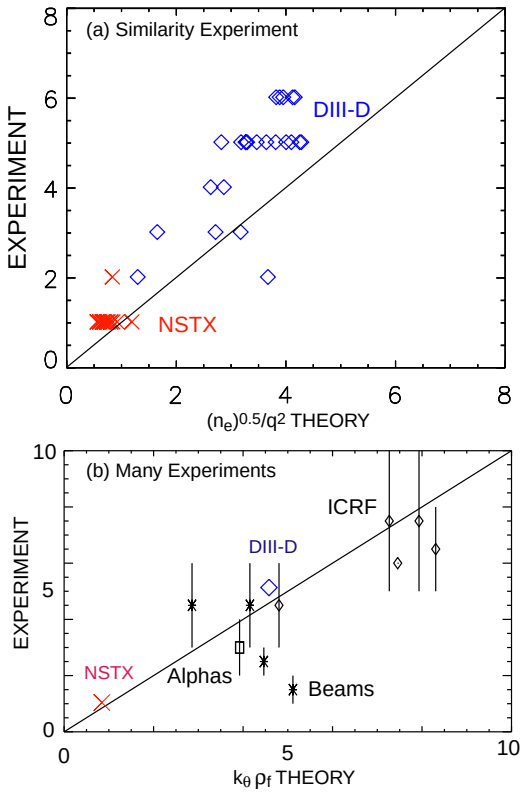

Figure 12. (a) Toroidal mode number of the strongest TAE in the magnetics spectrum versus $\sqrt{n_e}/q^2$ for the database of NSTX ($\times$) and DIII-D($\diamondsuit$) discharges. The theory is 1.3 times Eq. 2, with n_e taken from an average central density measurement and $q = 0.8q_0 + 0.2q_{95}$. (q_{95} is the value of q at the surface that encloses 95% of the poloidal flux.) (b) Most unstable toroidal mode number versus Eq. 1 for many experiments (from Ref. [14]), with a typical NSTX ($\times$) and DIII-D ($\diamondsuit$) point from the present experiment included in the figure.

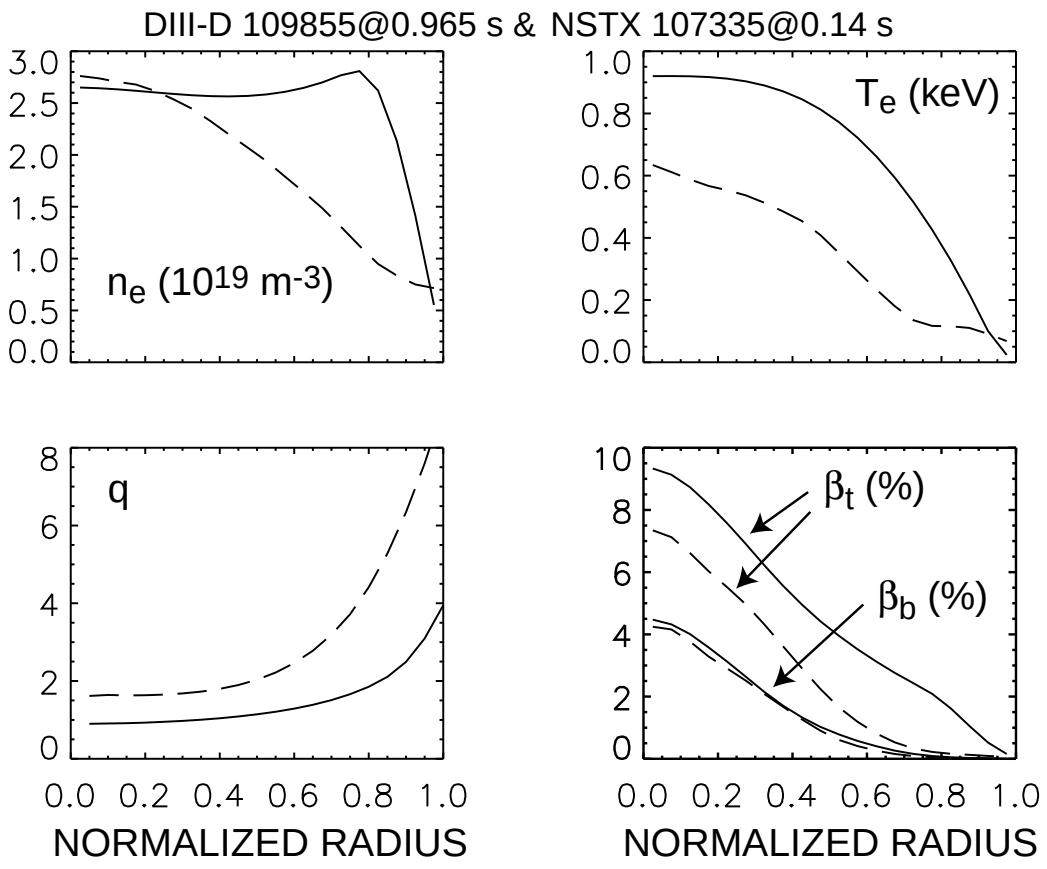

Figure 13. Radial profiles of electron density and temperature, safety factor, and the total toroidal and beam betas for the NSTX (dashed line) and DIII-D (solid line) cases selected for detailed theoretical analysis. DIII-D (NSTX) parameters: $B_T(0) = 0.62$ (0.50) T; $I_p = 0.57$ (0.84) MA; $R(0) = 1.69$ (0.87) m; $a = 0.60$ (0.59) m; $\kappa = 1.80$ (1.65); $\delta = 0.41$ (0.38); $P_B = 2.2$ (1.7) MW.

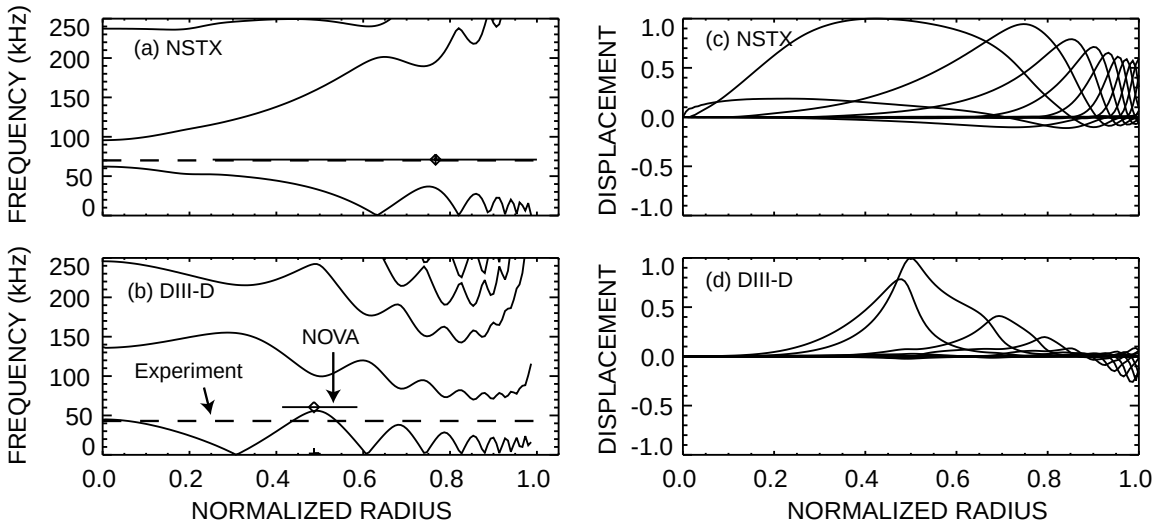

Figure 14. (a) $n = 1$ Alfvén continuum in NSTX discharge #107335 at 0.14 s and (b) $n = 3$ Alfvén continuum in DIII-D discharge #109855 at 0.965 s. The dashed line is the measured frequency in the plasma frame inferred from the magnetics spectra and the solid line with the diamond represents the frequency of the unstable TAE calculated by NOVA-K. The corresponding mode structure for poloidal harmonics (c) $m = 0$-15 in NSTX and (d) $m = 1$-16 in DIII-D.

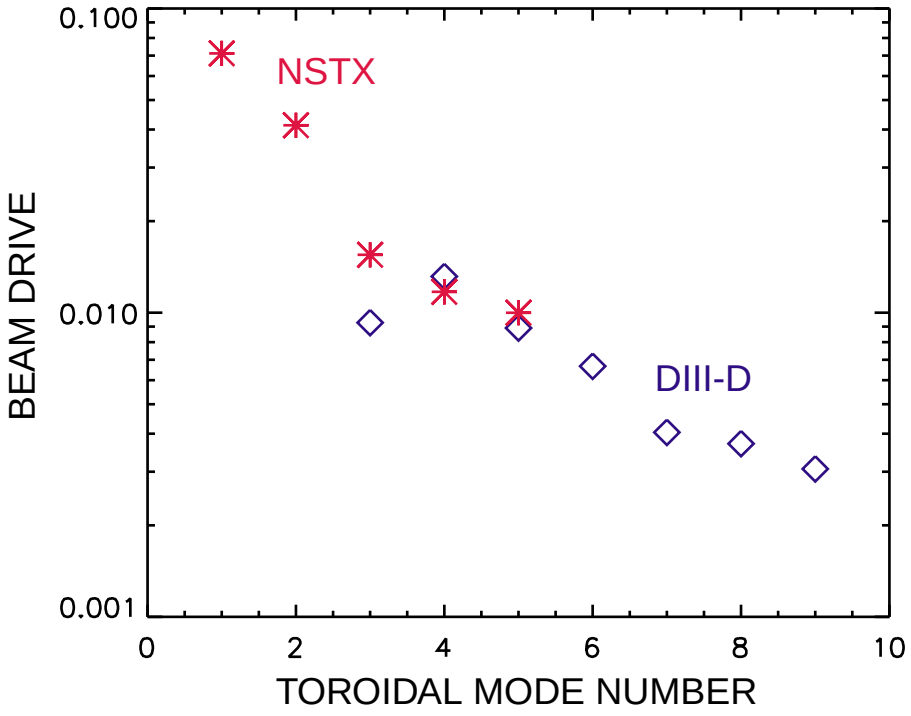

Figure 15. Beam-ion drive for the most unstable TAE calculated by NOVA-K as a function of toroidal mode number for the NSTX ($\times$) and DIII-D ($\diamondsuit$) cases shown in Fig. 13. The calculation includes finite drift orbit and finite gyroradius effects.

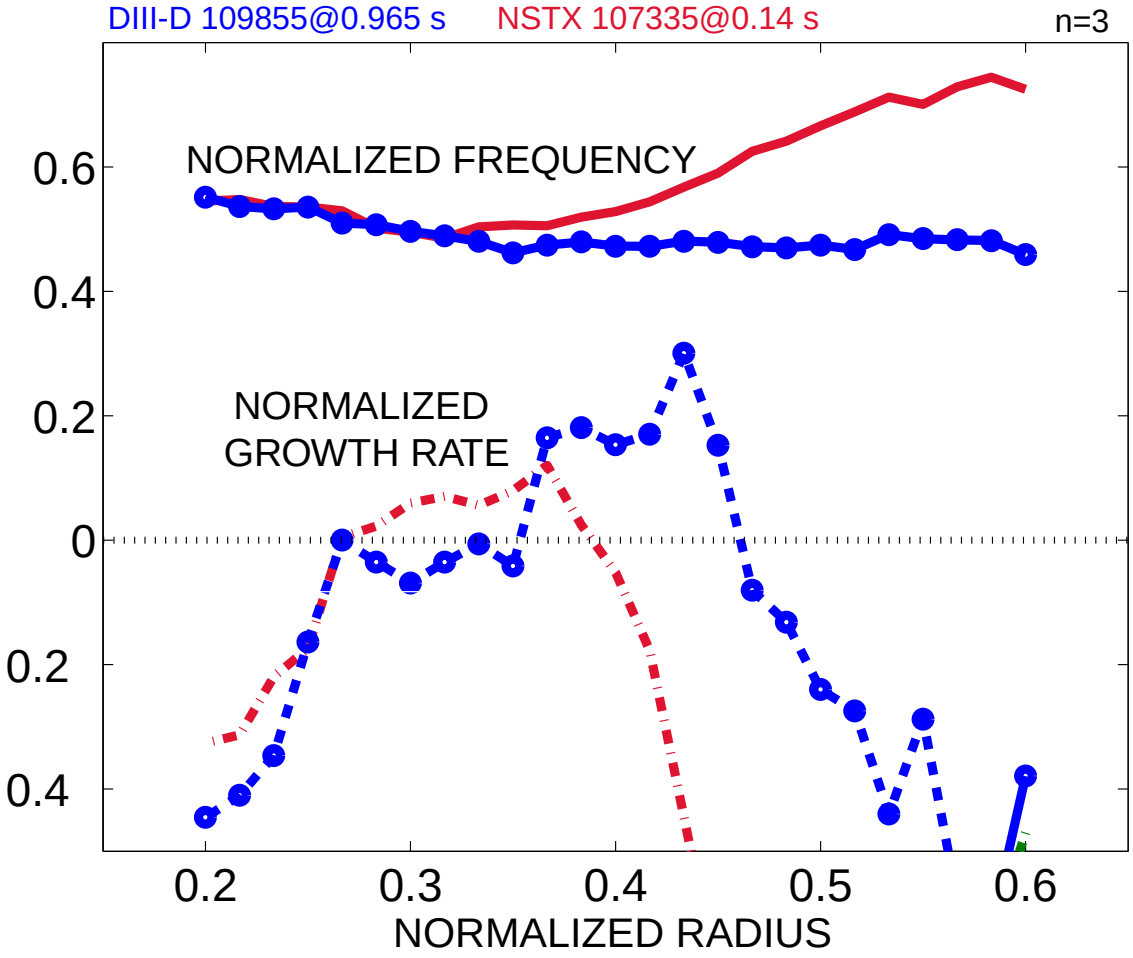

Figure 16. Frequency and growth rate (normalized to the central Alfvén frequency v_A/qR) for the DIII-D (circles) and NSTX (no symbols) cases versus the normalized square root of the toroidal flux as calculated by HINST for $n = 3$.

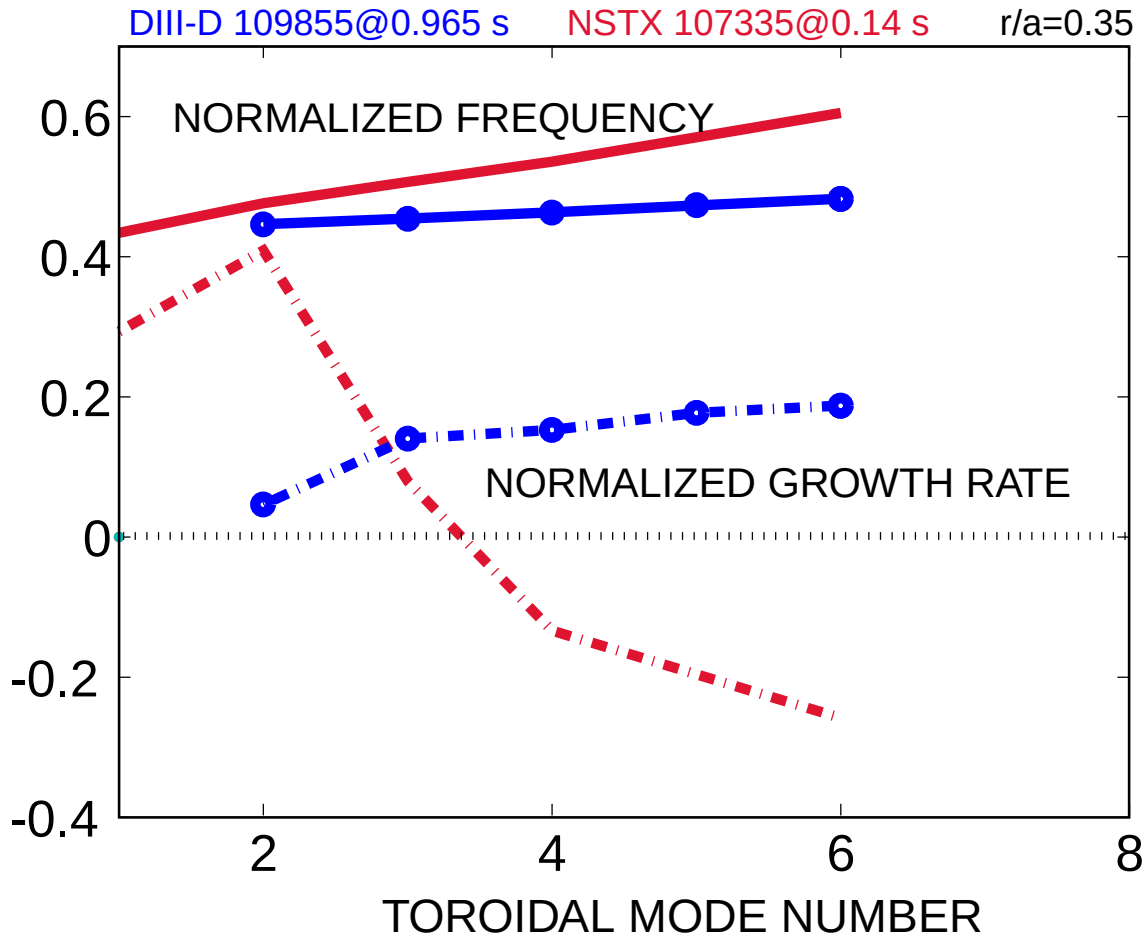

Figure 17. HINST calculation of frequency and growth rate for the DIII-D (circles) and NSTX (no symbols) cases versus toroidal mode number for a normalized radius of 0.35.